e-Prime - Advances in Electrical Engineering, Electronics and Energy 9 (2024) 100649

Contents lists available at ScienceDirect

e-Prime - Advances in Electrical Engineering, Electronics and Energy

journal homepage: www.elsevier.com/locate/prime

Design and investigation of high power quality PV fed DC-DC boost converter

Khadiza Akter [a,b,*], S.M.A. Motakabber [a], A.H.M. Zahirul Alam [a], Siti Hajar Binti Yusoff [a]

[a] Electrical and Computer Engineering, International Islamic University Malaysia, Malaysia
[b] Electrical and Electronics Engineering, International University of Business Agriculture and Technology, Bangladesh

ARTICLE INFO

Keywords:
MPPT Controller
Particle Swarm Optimization (PSO)
Artificial Neural Network (ANN), DC-DC Converter, High Voltage Gain (HVD), Low Voltage Stress (LVS), High Efficiency

ABSTRACT

This study presents a new improved voltage gain dc-dc converter architecture to maximize solar photovoltaic (PV) power output. The maximum power point tracking (MPPT) method utilizes particle swarm optimization (PSO)–based artificial neural networks (ANN) to reduce the oscillations of output electrical performance at the maximum power point (MPP). For any solar cell temperature and irradiance, the ANN delivers the electrical current and voltage outputs at the MPP and thus could reach the MPP in minimum instances. A DC-DC converter needs specific characteristics to work with photovoltaic systems. These include higher voltage development to meet increased DC link voltage requirements, the continuous input current to extend the PV system life, common grounding to prevent electromagnetic interference, and reduced electrical stress with fewer components. This paper combines a quasi-switched switch inductor network and extendable diode capacitor modules to achieve the quality mentioned earlier. The converter offers constant input current, high efficiency (95 %) with considerable gain (12 times higher than input), lower voltage stress (almost one-fifth of output voltage), and a common grounding feature. The effectiveness of the proposed MPPT technique is analyzed in terms of higher efficiency, MPP tracking time, gain, and the normalized voltage stress on diodes. The experimental step is developed to validate the simulation (Simulink and Psim) results of the present research work.

1. Introduction

Due to the high installation cost and low energy conversion efficiency of solar photovoltaic (SPV) systems, tracking the maximum power from the PV panel and transmitting it to the load is essential to maximizing the effectiveness of the SPV system. PV panels reach their peak power at a specific operating point when the power change rate concerning voltage is zero [1]. It can be monitored by connecting an appropriate DC-DC converter to a photovoltaic panel and using the MPPT algorithm to operate the switch to calibrate the impedance. High tracking precision and reliable steady-state and transient performance are often significant factors to consider when assessing the effectiveness of MPPT approaches. To meet these requirements, various MPPT approaches have been explored in the literature [2–7]. A traditional algorithm called perturb & observed (P&O) determines the PV module's maximum power. However, there is fluctuation around the MPP in the P&O algorithm output [8]. An approach to the P&O algorithm problem is the Incremental Conductance (IC) method. It stops the fluctuation near the MPP and increases effectiveness. The authors have developed the MPPT approach known as the delta P&O approach [9], and an adjustable step size is advised for enhancing MPPT. The MPPT technique is created in [8] using voltage and duty cycle perturbations.

The fuzzy logic controller-based P&O algorithm was proposed in [10] and investigated with different sun irradiance conditions to achieve true MPP. Since PV voltage is detected and cell temperature is predicted using the current-sensorless MPPT technique [11], PV current can be computed using a predetermined look-up table [12]. However, this method has reliability and complexity issues due to the precision of the model and the challenges of estimating the ambient temperature. One current sensor can be skipped as a novelty claimed, as suggested in [13]. The PV voltage (V_{PV}) and output-inductor-current (I_L), two observable states, are used to estimate the PV current sensor value. To enhance the efficiency, closure rate, and steady-state fluctuation of MPP tracking under variable weather circumstances, P&O/IC algorithms are integrated with ANN/FLC. However, the many peaks generated in the method made it ineffective under PSC. AS metaheuristic algorithms can regulate the nonlinear curve without requiring derivative information, they are utilized to monitor the global MPPT even in changing weather

* Corresponding author.
E-mail address: khadiza@iubat.edu (K. Akter).

https://doi.org/10.1016/j.prime.2024.100649
Received 6 July 2023; Received in revised form 6 June 2024; Accepted 15 June 2024
Available online 16 June 2024

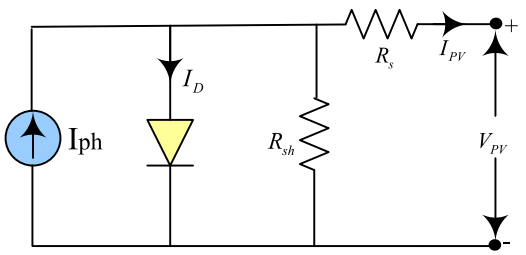

Fig. 1. PV cell single diode model.

conditions. However, the appropriate adjustment of parameters has a significant impact on the overall effectiveness of metaheuristic algorithms. An essential role for ANN can be played in developing MPPT for the solar system in PSC. More correctly, ANN forecasts the PV system's nonlinear behavior. Tracking speed will be increased by combining the PSO method with ANN implementation. Additionally, this method may identify MPP more consistently than other hybrid methods since it incorporates the PSO algorithm.

Interfacing DC-DC converters are essential for converting low-level PV voltage sources to consistent high-level DC voltages and, at the same time, tracking the highest MPP. Since it determines the input ripple factor and offers a variety of voltage transformation ratios, choosing a DC-DC converter is also crucial for tracking the MPP. Traditional boost converters provide an infinite boosting proportion, although this is not always the case in practice [14]. Different DC-DC converter configurations have been proposed in prior studies and reported by the authors. A non-isolated DC/DC converter called a cascaded converter [15] raises low input voltage without utilizing a large duty cycle. On the other hand, because of the high voltage stress, an extremely robust switch is needed. Large boosting ratios can be achieved using switched capacitors and switched inductor topologies without requiring a large duty cycle [16,17].

Another improvement to attain excellent step-up capabilities is the voltage-lift approach. It has several benefits, including high voltage gain and low potential stress on the operating device [18–20]. However, many diode-capacitor processes are needed when the transformation ratio is very high [17,19]. SI-based transformerless topology is described in [21] and can produce a theoretical raising of ((1+d)/ (1-d)). Voltage stress is approximately equivalent to output voltage, yet switches undergo exposure to high voltages. Similarly, its semiconductors are under excessive voltage stress, which could reduce system efficiency. It is mentioned in [22] that a modified SEPIC converter has a somewhat higher gain than a boost converter. In [23] reports a converter with an enhancement of (5+D)/(1-D), wherein D is the duty-cycle ratio. Both of these converters have pulsating input current and no common ground. Quadratic boost converters are used to increase the gain [24]. In [25] and [26], converters with gains of (2+D)/(1-D)2 and (3- 2D)/(1-D)2, respectively, are described. When the duty ratio exceeds 70 %, the quadratic converters gain more. As a result, inductor core saturation is a severe issue in converters that operate at high frequencies. Various converters with substantial gain at lower duty ratios are given in the literature [26–31] to prevent such saturation problems.

In [32], it employs a passive switching inductor-capacitor network. However, it contains extra components, erratic input current, and no shared ground. Recently, switched capacitors, switched inductors, or other voltage-boosting topologies have been utilized in conjunction with Z-source (ZS) and Quasi-z-source (Q-ZS) networks to boost the voltage gain [33–35]. Moreover, a switch capacitor-utilized ZS/Q-ZS converter is reported. The converters achieve Higher voltage gain [34], but additional components, including three inductors, are used. The electrical power density of the converter diminishes when more inductors are used. Gain is increased by combining a pair of switch-based switching capacitors with various boosting circuits [36–38]. Like traditional Q-ZS, the converter in [39] excludes common ground and has a pulsating input current. To ensure the proper functioning of DC-DC converter with MPPT at reduced switching loss, non pulsating supply current, low voltage stress on semiconductor components, minimal reverse recovery losses of diodes along with high voltage transformation ratio is crucial, and the development of such an approach is still under research. In addition, with a high-power quality converter, the development of a well-performed MPPT is also a big concern. A single-switched quasi-structured high gain extensible boost converter is suggested hereto solve the aforementioned negative aspects. The proposed configuration includes common ground, continuous input current with minimal ripple contents, higher voltage gain at varying duty ratios, remarkably reduced voltage stress on semiconductors, and high efficacy with an MPPT controller. With increased efficiency, it can deliver 432 V from a 32 V input at a 40 % duty ratio. The recommended converter's key component is a switched capacitor circuit at the input, which helps to boost voltage gain. Furthermore, the recommended converter will have a constant input current and a common ground between the power source and the load. The proposed topology is efficiently incorporated as a solar interfacing circuit extracting the optimum output of the PV source.

1.1. Novelty of work

This study innovatively presents set-theoretic research and thorough performance evaluation by focusing on critical aspects of two selected MPPT techniques. The distinctive elements of this study include:

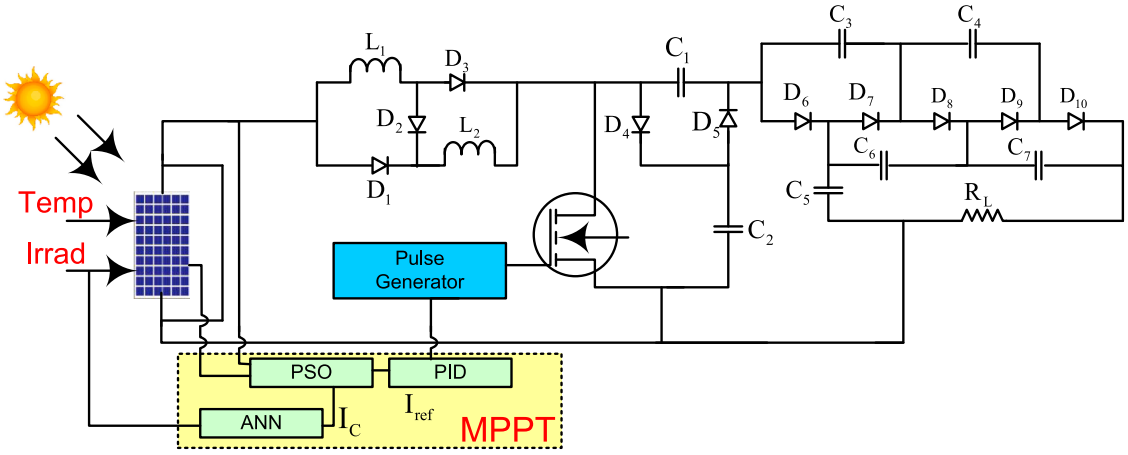

Fig. 2. Block diagram for the hybrid approach

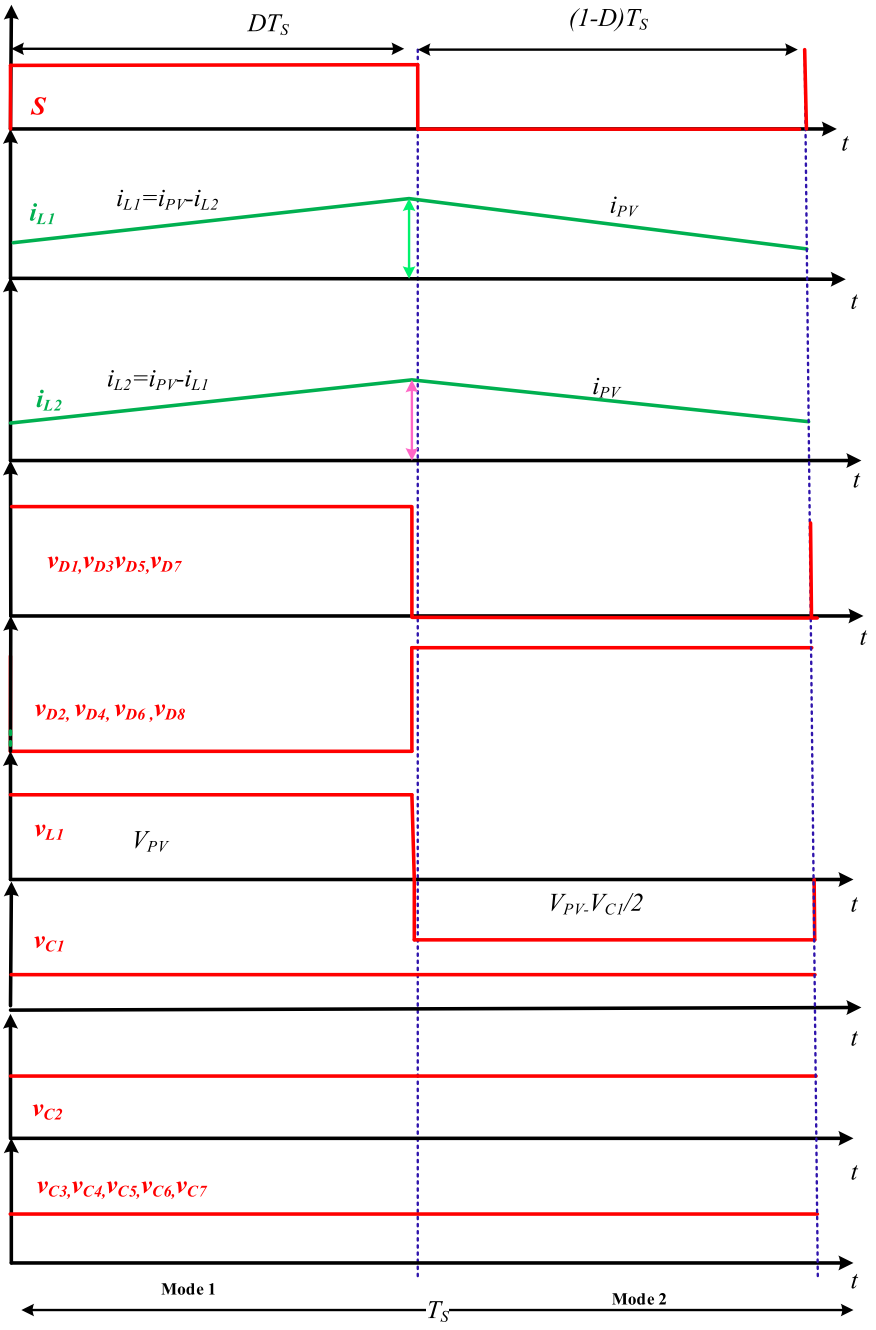

Fig. 3. Theoretical waveform of proposed topology

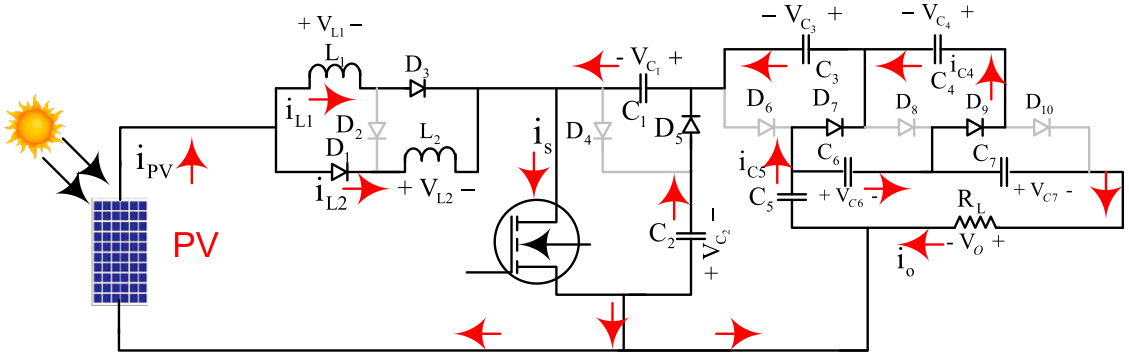

Fig. 4. Functionality of the proposed converter when the switch is conducting.

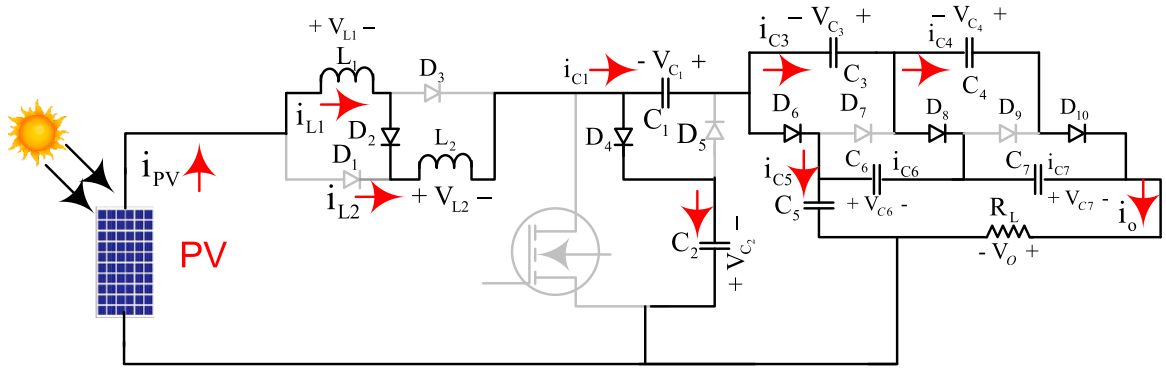

Fig. 5. Functionality of the proposed converter when the switch is not conducting.

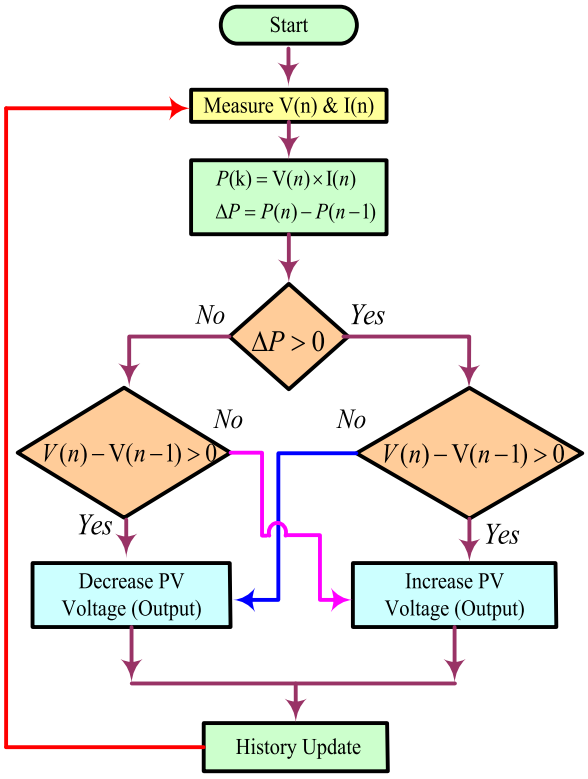

Fig. 6. Conventional P&O-based MPPT algorithm flowchart [49].

- A thorough comparison of the transitory performances of two separate MPPT methods, namely P&O and PSO-ANN, allows for an exhaustive evaluation.
- To ensure the correct execution of the MPPT algorithm, each approach is tested with a DC-DC converter, which is a commercially available tool. On top of that, we conduct a thorough performance analysis.
- PSO-ANN outperforms the traditional P&O-based MPPT method in real-time comparisons and experimental validations concerning tracking time, efficiency, computational complexity, and higher system output power and current.
- The proposed DC-DC converter provides high transformation efficiency, reducing semiconductor voltage stress

This paper is further structured into sections as follows: Section 1 illustrates the introduction and novelty of the work. Section 2 explains the PV system technology and DC-DC converter methodology. Section 3 demonstrates both the MPPT approaches chosen to study their transient

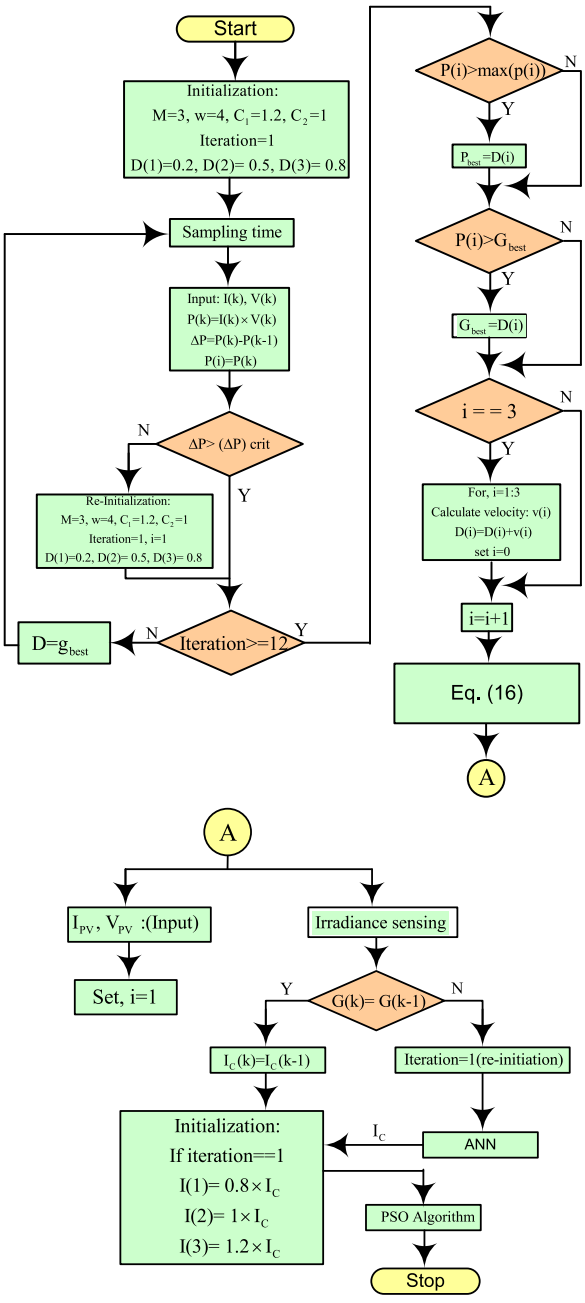

Fig. 7. Flowchart of PSO-trained ANN.

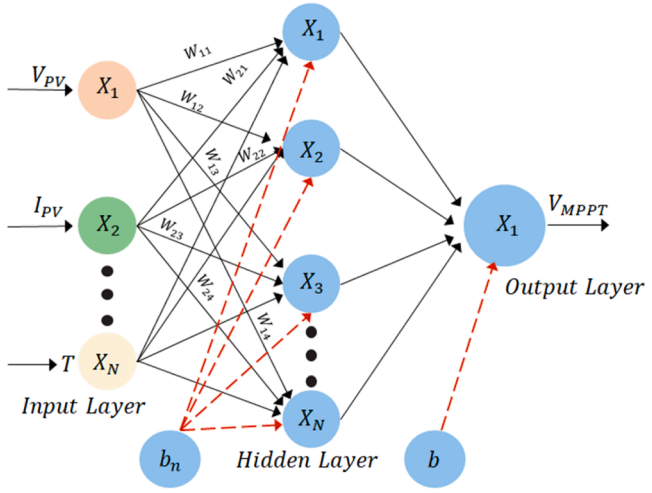

Fig. 8. ANN structure.

Table 1
Specification of ANN.

Hidden layers	1
Activation Function	Sigmoidal
Loss Function	MSE
Learning Rates	0.001
Batch Size	05
Learning Algorithm	Stochastic gradient descent (SGD)

Table 2
Training parameters of ANN.

Parameter	Value
Maximum Power (P_m)	175.09 W
Open circuit voltage (V_{OC})	43.99V
Short circuit current (I_{SC})	5.17A
Current at maximum power (I_m)	4.78A
Voltage at maximum power (V_m)	36.63V
Voc temperature coefficient	-0.3616
Ioc temperature coefficient	0.0415
ANN type	Feedforward network
No. of layers	2
No.of neuron	10
Training	Levenberg marquardt

responses. In addition, a comparative study and results for MATLAB/Simulink and experimental studies are shown in Sections 4–5. Furthermore, Section 6 concludes the outcomes of the present study.

2. PV system technolgy and DC-DC converter topology

Fig. 1 depicts the standard single diode model of PV module. In a mathematical model of the PV cell operating under uniform irradiance, the current-voltage relation can be expressed using Eq. (1) as,

$$I_{PV} - I_{ph} - I_D - \frac{V_{PV} + I_{PV}R_S}{R_{Sh}} \tag{1}$$

By arranging the PV cell through the series and parallel connection and expressed in the Eq. (2). Moreover, Shockley Eq. (3) is helpful to assess the current values through the diode as follows,

$$\left.\begin{aligned} I_{PV} &= N_P I_{ph} - N_s I_D - \frac{V_{PV} + I_{PV}R_s n_r}{R_{sh} n_r} \\ n_r &= \frac{N_s}{N_P} \end{aligned}\right\} \tag{2}$$

$$I_D = I_o\left(e^{\frac{q(V_{PV}+I_{PV}R_s)}{AKTN_s}} - 1\right) \tag{3}$$

Fig. 2 depicts a non-isolated high-raise DC-DC converter is used in PV applications.

This figure demonstrates how the converter can enhance the voltage level of RES and track the MPP of PV panels, enabling them to be connected to a high-voltage DC. Solar PV voltage is delivered to the proposed DC-DC converter by limiting the fluctuations in frequency and duty cycles. The proposed topology consists of SI (L_1, L_2, D_1, D_2 and D_3) and a quasi-switched network (D_4, D_5, C_1 and C_2) at the switching side. The circuit's output voltage can be extended to any desired level, expanding the number of diodes and capacitors. Depending on the switch status of S = 0 or 1, the converter has two distinct modes of operation in continuous conduction mode (CCM). The examination of operation modes is looked into in the following sections, while ideal circuit component characteristics are considered. Fig. 3 shows the converter's operational waveforms.

2.1. State 1. $0 \le t \le DT_S$

Mode I occurs, because the switches are activated by an intense PWM signal, as shown in Fig. 4 Diodes D_2, D_4, D_6, D_8, and D_{10}, are switched off after the switch is powered on. On the other hand, D_1, D_3, D_5, D_7, and D_9 are conducted because they are forward-biased. Inductors L_1 and L_2 are, therefore, filling energy from the DC source. L_1 and L_2 are charged in parallel since they have the same magnitude and share the same current. There is a parallel connection between the capacitors C_1 and C_2. As a result, V_{C2} has the same voltage as V_{C1}. The capacitor C_5 fills the charge to the capacitor C_3. Capacitor C_6 charges C_4, hence V_{C6} is equal to V_{C4}. Capacitor C_4 provides the power for the load.

Since L_1=L_2=L therefore $V_{L1} = V_{L2}$, applying KVL in Fig. 4 and expressed in Eq. (4)-(5) as follows,

$$V_L = V_{PV} \tag{4}$$

$$\begin{cases} V_{C1} = V_{C2} \\ V_{C6} = V_{C4} \\ V_{C5} = V_{C2} - V_{C3} \\ V_O = V_{C5} + V_{C6} + V_{C7} \end{cases} \tag{5}$$

Additionally, the subsequent current equations are produced by using the Kirchhoff current law (KCL) in Fig. 4 and expressed in Eq. (6) as follows,

$$\begin{cases} i_{PV} = i_{L1} + i_{L2} \\ i_S = i_{PV} + i_{C1} \\ i_{C2} + i_{C3} = i_{C1} \\ i_{C5} = i_{C6} + i_{D6} \\ i_{C6} = i_{C7} + i_{C4} \\ i_{C7} = i_o \end{cases} \tag{6}$$

2.2. State 2. $0 \le t \le (1\text{-}D)\ T_S$

For CCM switch S is off when the circuit is not operating in a shoot-through state. During this state Diodes D_1, D_3, D_5, D_7, and D_7 are non-conducting and rest are conducting as depicted in Fig. 5.

Through the total voltage V_{in} + V_L, the capacitors C_1 and C_2 are charged. Capacitor C_5 gets charged from C_1 and C_2. In the output side C_6, C_3 and C_7, C_4 are connected in parallel. The KVL in Fig. 5. is applied to produce the Eq. (7) as given below.

$$\begin{aligned} V_{L1} &= V_{L2} \\ V_{L1} + V_{L2} &= V_{PV} - V_{C2} \\ 2V_L &= V_{PV} - V_{C2} \\ V_L &= \frac{V_{PV} - V_{C2}}{2} \end{aligned} \tag{7}$$

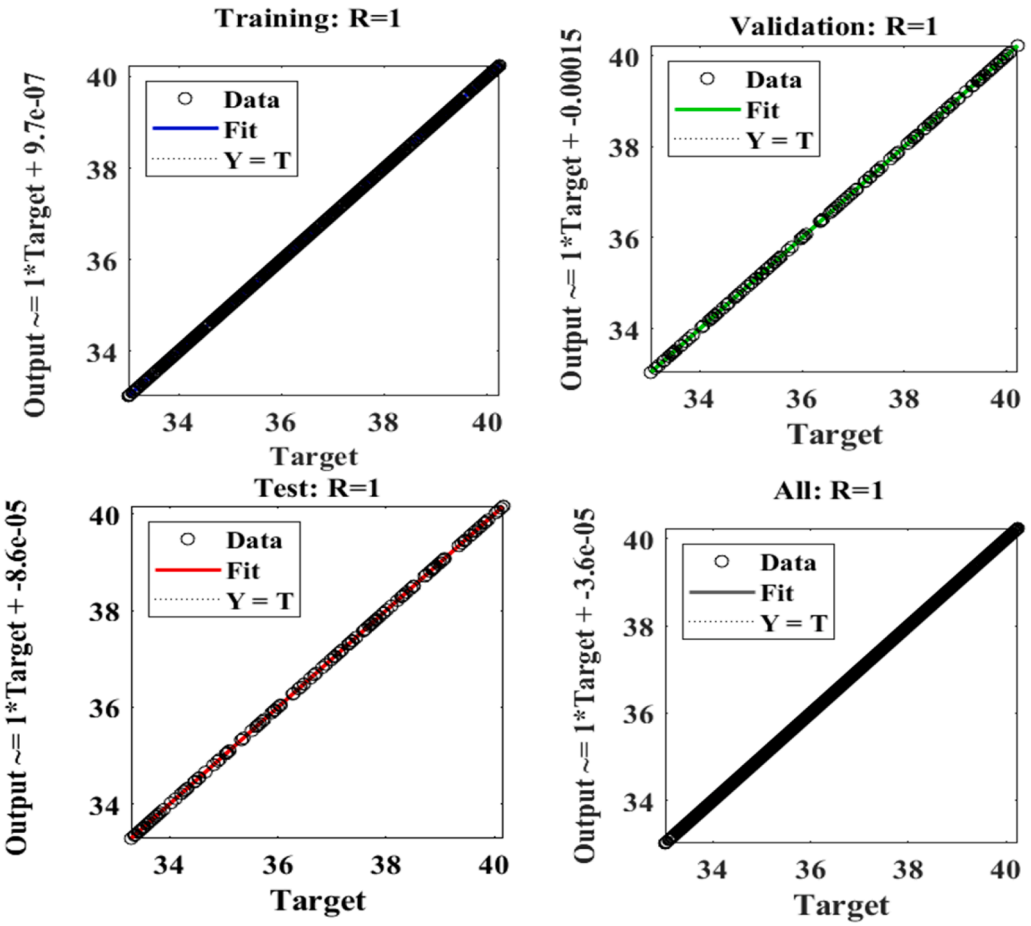

Fig. 9. Performance of ANN during training for the hybrid approach.

Moreover, applying KCL and expressed in Eq. (8) as follows,

$$\begin{cases} i_{L1} = i_{L2} = i_{PV} \\ i_{C1} = i_{PV} - i_{C2} \\ i_{C3} = i_{C4} - i_{D7} \\ i_{C5} = i_{D5} - i_{C6} \\ i_{C4} = i_{C7} - i_o \\ i_{C7} = i_{C4} - i_o \end{cases} \tag{8}$$

Non-Shoot Through State for DCM is expressed in Eq. (9) as,

$$\begin{cases} V_{C1} + V_{C2} = V_{C5} \\ V_{C3} = V_{C6} \\ V_{C4} = V_{C7} \\ V_O = 3V_{C7} \end{cases} \tag{9}$$

2.3. Analysis of voltage gain

Using the inductor volt-second balancing theorem across one switching period to L. Where L_1=L_2=L. With the help of Eq. (4) and (7) voltage gain equition can be derived.

$$\int_0^{DT_S} V_L dt + \int_{DT_S}^{T_S} V_L dt = 0 \tag{10}$$

$$\begin{cases} V_{PV}DT_S + \dfrac{(V_{PV} - V_{C2})(T_s - DT_S)}{2} = 0 \\ V_{PV}DT_s + \dfrac{V_{PV}T_S - V_{PV}DT_S - V_{C2}T_S + V_{C2}DT_S}{2} = 0 \\ 2V_{PV}DT_S + V_{PV}T_S - V_{PV}DT_S - V_{C2}T_S + V_{C2}DT_S = 0 \\ DV_{PV} + V_{PV} - V_{C2} + DV_{C2} = o \\ V_{PV}(1+D) - V_{C2}(1-D) = 0 \\ V_{C2}(1-D) = V_{PV}(1+D) \\ V_{C2} = \dfrac{V_{PV}(1+D)}{(1-D)} \begin{cases} V_{C2} = \dfrac{V_{C5}}{2} \\ V_O = 3V_{C5} \end{cases} \\ V_O = \dfrac{6V_{PV}(1+D)}{(1-D)} \end{cases} \tag{11}$$

Design of Inductor, Since $L = L_1 = L_2$

$$\begin{cases} L_1 \dfrac{dI_{L1}}{dt} = V_{PV} \\ \dfrac{dI_{L1}}{dt} = \dfrac{V_{PV}}{L_1} \\ \dfrac{\Delta I_{L1}}{DT_S} = \dfrac{V_{PV}}{L_1} \\ L_1 = \dfrac{(V_{PV})D}{I_L F_S \Delta I_L} \end{cases} \tag{12}$$

Where $T_S = \frac{1}{F_S}$, Design of capacitor

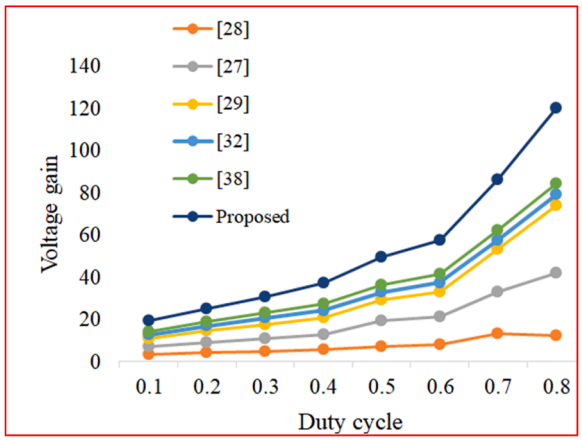

(a)

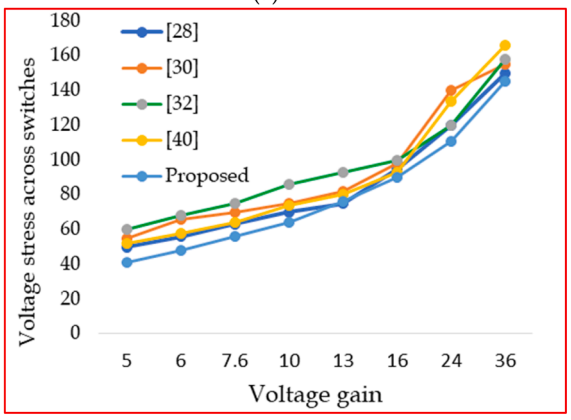

(b)

Fig. 10. (a) Voltage gain comparison (b) switching stress comparison of various topolgy.

$$\begin{cases} I_{C1} = C_1 \dfrac{dV_{C1}}{dt} = \dfrac{V_o}{R(1-3D)} \\ C_1 = \dfrac{3V_{in}D}{R(1-3D)\Delta V_{C1} F_S} \end{cases} \tag{13}$$

2.4. Voltage stress across semiconductors

Individual semiconductor components experience voltage stress when turned off or reverse-biased. This information is used to compute the voltage across various semiconductor devices. In the first operating mode, voltage stress across reverse biased diodes can be derived using Eq. (14)-(15) as,

$$\begin{cases} V_{D2} = V_{L1} = V_{PV} \\ V_{D4} = V_{C2} = \dfrac{V_{PV}(1+D)}{(1-D)} \\ V_{D6} = V_{C3} = -\dfrac{V_{PV}(1+D)}{(1-D)} \\ V_{D8} = V_{C4} = V_{C6} = \dfrac{V_{PV}(1+D)}{(1-D)} \\ V_{D10} = V_{C7} = \dfrac{V_{PV}(1+D)}{(1-D)} \end{cases} \tag{14}$$

In second operating mode voltage stress across reverse biased diodes are

$$\begin{cases} V_{D1} = V_{D3} = V_L = V_{PV} \\ V_S = V_{C2} = \dfrac{V_{PV}(1+D)}{(1-D)} \\ V_{D5} = V_{C1} = \dfrac{V_{PV}(1+D)}{(1-D)} \\ V_{D7} = V_{C3} = \dfrac{V_{PV}(1+D)}{(1-D)} \\ V_{D9} = V_{C4} = \dfrac{V_{PV}(1+D)}{(1-D)} \end{cases} \tag{15}$$

3. MPPT techniques

3.1. Conventional P&O based MPPT

In terms of tracking MPP, this approach is by far the most used. The P&O approach is tweaked slightly to change the PV module's power output. Constant comparisons are made between the output power and the previous power. The procedure is carried out again and again until either the PV output power increases or the perturbation is reversed. This technique makes use of modifying the PV module's voltage. One way to tell if power has gone up or down is to play around with the voltage and see what happens to the output. The operating point of the PV module moves to the left of the MPP if raising the voltage increases power. Therefore, in order to get close to the MPP, further changes in the direction of higher voltages are required. The operational point of the PV module is located to the right of the MPP if, on the other hand, power drops as voltage increases. In this instance, in order to obtain the MPP,

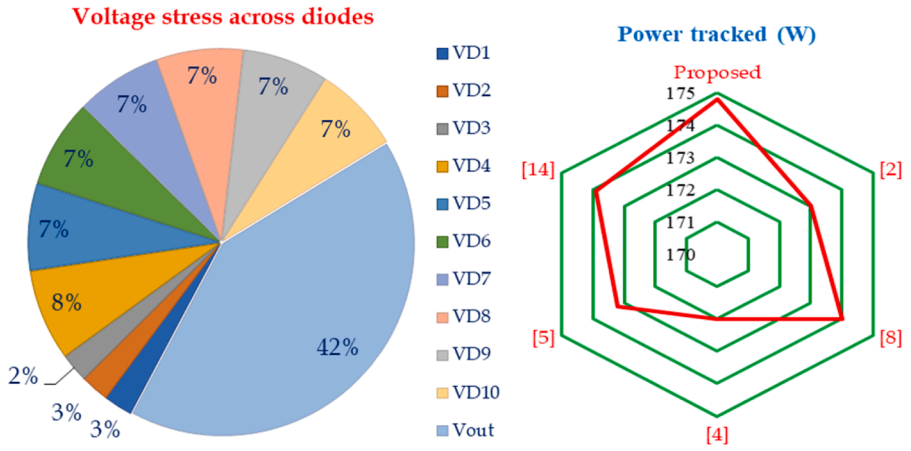

(a) (b)

Fig. 11. (a) Percentage of the stress of diodes used in proposed topology (b) and MPP tracking comparison.

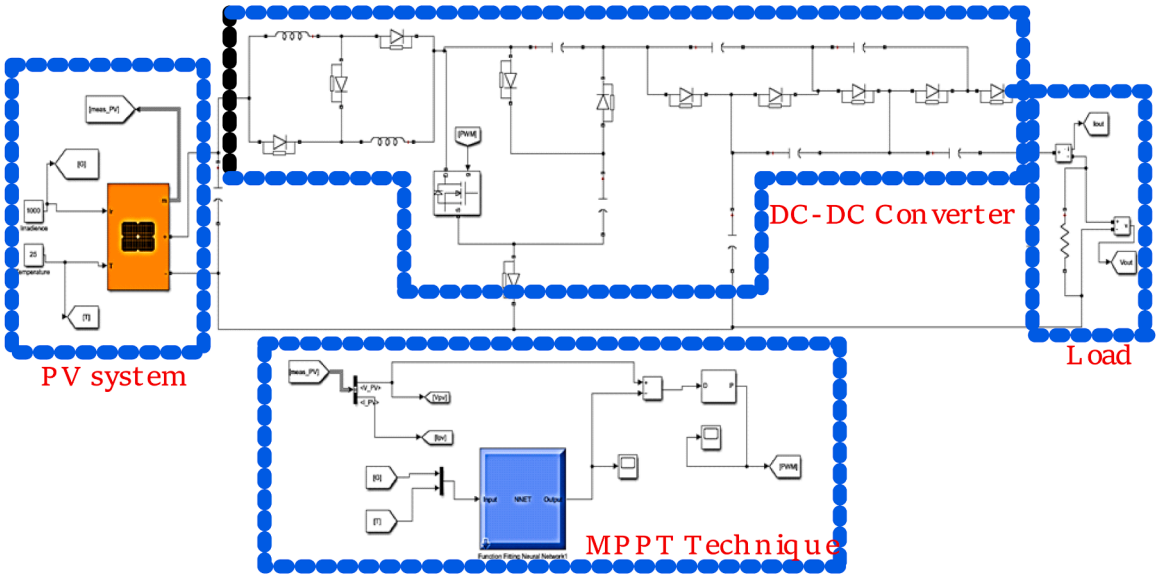

Fig. 12. Simulink model of MPPT assisted PV system.

Table 3
Comparison studies of high-performance converters in recent year.

Topology	No. of components	Voltage stress on switch	Voltage stress on diode	Efficiency (%)	Switching frequency	Voltage gain	Tested power	Switching technique	Input current ripple	Common ground
[45]	12	$\frac{1}{1+N+D}\frac{1-D}{1+N+D}$	$\frac{1+N}{1+N+D}$	94.4 %	50kHZ	$\frac{1+N+D}{(1+D)^2}$	400W	NA	Continuous and less	Yes
[46]	18	$\frac{1}{2N+2}$	$\frac{2}{2N+2}$	96.7 %	118kHZ	$\frac{2N+2}{1-D}$	400W	ZCS	Continuous and less	No
[47]	16	$\frac{V_o}{2N+4}$	$\frac{2N}{2N+4}$	95.8 %	40kHZ	$\frac{2N+4}{1-D}$	200W	ZCS	Continuous and less	No
[48]	13	$\frac{V_o}{3N+1}$	$\frac{2NV_o}{3N+1}$	97 %	50kHZ	$\frac{3N+1}{1+D}$	400W	ZCS	Continuous and less	Yes
[27]	16	$\frac{V_O}{5}$	$\frac{2V_O}{5}$	95.5 %	50kHZ	$\frac{5}{1-2D}$	500W	NA	Continuous and less	Yes
[35]	14	$\frac{1}{3-2D}$	$\frac{1}{3-2D}$	91.25 %	100kHZ	$\frac{3-2D}{1-2D}$	400W	NA	Continuous and less	Yes
Proposed	20	$\frac{V_{PV}(1+D)}{(1-D)}$	$\frac{V_{PV}(1+D)}{(1-D)}$	95 %	40kHZ	$\frac{6V_{PV}(1+D)}{(1-D)}$	550W	ZVS	Continuous and less	Yes

changes geared towards lower voltages are required. Fig. 6 shows the P&O algorithm flowchart for execution, and the given steps are to be followed to achieve the MPP [49],

Step-1: Initially measure I_{PV} and V_{PV} at any instant 'n'

Step-2: Calculate the P_{PV} at 'n' & ΔP is assessed by comparing the power at instance 'n' & conventional power at '$n-1$'
Step-3: Check $\Delta P > 0$ or not using algorithm.

- If above statement is true, then check for $V(n) - V(n-1) > 0$ or not.
  If Yes, V_{PV} is increased If No, V_{PV} is decreased
- If above statement is false, check for $V(n) - V(n-1) > 0$ or not.
  If Yes, V_{PV} is decreased If No, V_{PV} is increased

Step-4: After restoring these variables, the system begins to search for MPP.

3.2. PSO-ANN-based MPPT

Over the past ten years, AI techniques have been widely deployed for MPP tracking in the photovoltaic power system. This is because, under partial shade conditions (PSCs), conventional MPPT algorithms cannot track the global maximum power point (GMPP). Compared to traditional MPPT techniques, all AI-based MPPT algorithms have quick convergence speeds, low steady-state fluctuation, and excellent efficiency. The naturally occurring neural networks found in animal brains inspire ANNs. Apply this technique and evaluate the nonlinearity of the P-V and I-V relationship. An artificial neural network (ANN) retrieves these inputs from the current and voltage, temperature, irradiance, and metrological data and continuously learns to adapt to the actions of the solar system for the highest amount of power.

The dataset is acquired from the simulation or hardware setup by feeding solar temperatures, irradiance PV current, and voltage into ANN and obtaining the matching Pmax or Vmaxat output. These data are transformed into training data and sent into the created ANN to train it. The test samples are used to assess the overall performance of the developed ANN after training, while the errors are fed back into the ANN to be further adjusted. The benefits of ANN include its outstanding accuracy in simulating non-linearity and its ability to solve problems without using models or prior information [40]. ANN may be used to model and forecast the solar power system's output power, increasing the tracking system's accuracy and speed [41]. It has been demonstrated to have a more rapid response time and a lower MPP oscillation.

The square error algorithm is used to calculate the error as its feedback adjustment [42]. However, an accurate, standardized, and appropriate training set of data is a crucial requirement for the ANN to function at its best without a significant training error. To overcome the limitation of ANN, ANN-PSO-based MPPT has been developed. For training purposes and to forecast the outcome for certain weather circumstances, ANN is trained using a previous dataset that may comprise different amounts of radiation levels, temperature, short circuit current,

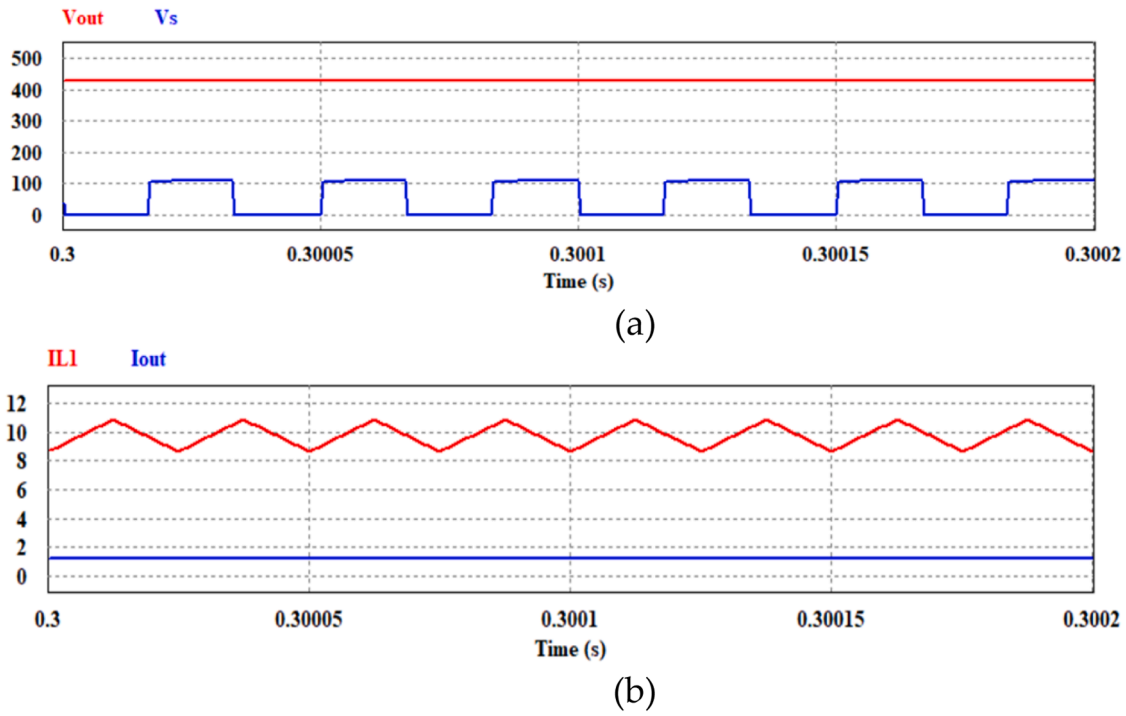

Fig. 13. Output voltage with respect o gate pulse voltage, (b) Output curent and inductor current waveform.

open circuit voltage, PV voltage, and PV current. In contrast, The PSO algorithm is essential for optimizing [40,43,44]. ANN provides the starting particle position for the PSO approach. The global MPP is not far from this initial particle size. Consequently, the PSO algorithm's range is limited. The PSO algorithm uses this initial value to determine the PV system at global MPP. And the PSO algorithm can now quickly locate the global MPP. Additionally, ANN recognizes any abrupt changes in solar irradiation and offers a new starting particle position for the PSO algorithm. Fig. 7 depicts the flow chart for this PSO trained ANN-based MPPT algorithm.

Below is a pseudo code for a PSO combined with an ANN based MPPT technique for a PV system. This method is used to optimize the efficiency of solar panels given steps are to be followed to achieve the MPP.

STEP-1: 1. Initialization

- Define the number of particles $(N_{particals})$
- Initialize particles' positions and velocities randomly within the PV module V & I values (permissible range).
- Initialize the ANN model with random weights.
- Set global best (g_{best}) and position best (P_{best}) for each particle.

STEP-2: Define Parameters

- Define learning rates for cognitive learning (C_1) and social learning(C_2).
- Set inertia weight (w) to control the particle velocity dynamics.

STEP-3: Main loop and evaluate the performance

- For each iteration i from 1 to $Max_{iterations}$
- For each particle j from 1 to $N_{particals}$
- ***Evaluate Performance***

  - Use current position (V & I) of particle '*j*' as input to the ANN.
  - Predict the power output using the ANN.
  - Update global best- If the fitness of current position is better than the fitness of P_{best} for particle 'j' update P_{best}.
  - Update global best g_{best}
  - Update velocity based on previous velocity, cognitive component (towards P_{best}), and social component (towards g_{best})

STEP-4: Training ANN

(*continued on next column*)

(*continued*)

STEP-1: 1. Initialization

- Use the best positions found (voltage/current) and corresponding power outputs as training data.
- Train the ANN to refine its prediction accuracy for power output.

STEP-5: Termination and output

- After reaching $(Max_{iterations})$ or if the change in g_{best} is minimal over several iterations, terminate the loop.
- Use the trained ANN and g_{best} position to control the PV power output.
- Return the optimal settings for V/I that correspond to g_{best}

PSO algorithm makes use of two operators such as (a) velocity update (b) particle position update. The capacity of the PV module determines both the optimal particle location and the velocity update. Finally, the algorithm's output is the boost converter switch's duty cycle. Consequently, in Eq. (16), represented the particle's location, which defines the duty cycle (D) as,

$$\left.\begin{aligned} D_i^{k+1} &= D_i^k + wv_i^k + c_1 r_1 \left(p_{besti} - s_i^k\right) \\ &+ c_2 r_2 \left(g_{besti} - s_i^k\right) \end{aligned}\right\} \tag{16}$$

3.3. ANN architecture, training process

An ANN, a distributed computing approach, may help keep track of data from experimental application systems. While expert knowledge is optional to model an application system, accurate data is needed to produce predictions of output functions that are as near to reality as feasible. This method converts the training data into a network with non-linear connections between nodes that provide input and output. The three main layers of a typical multilayer feed-forward ANN are input, hidden, and output, as shown in Fig. 8. Also, the weighting of connections between neurons and biases carried over from previous levels creates interconnections among the neurons in each layer. Using an artificial neural network (ANN), it can regulate the duty cycle by designing a network with a single hidden layer and activation functions such as sigmoid. This will give the output maps accurately to the range of 0 to 1. Utilize the mean squared error (MSE) loss function to get

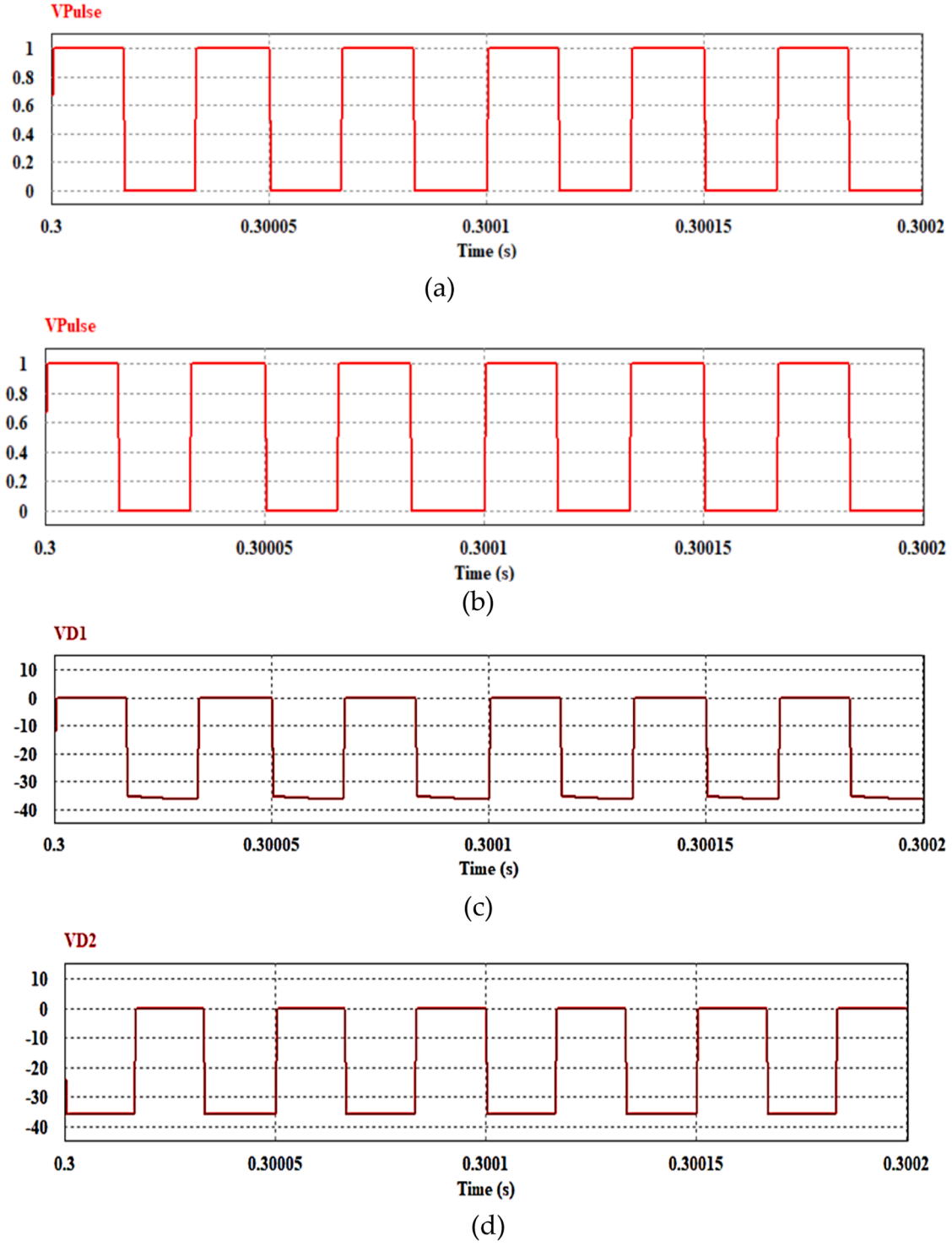

Fig. 14. Simulated output of various compnents(a)PWM pulse (c) voltage across D_1 (d) voltage across D_2 (e)voltage across D_3 (f) voltage across D_4 (g) voltage across D_5 (h) voltage across D_6 (i) voltage across D_7 (j) voltage across D_8(k) voltage across D_9 (l) Current through D_{10} (m) Current through D_2 (m) Current through D_2.

optimal results in any regression analysis. The initial learning rate is around 0.001; if required, it may change using adaptive schedules. A batch size that strikes a compromise between convergence speed and the results' generalization is 5. Optimization methods such as Adam, which adjusts the learning rate for each parameter and needs less tweaking than classic SGD, are used. The use of neural networks in this technique provides a solid framework for efficient duty cycle regulation. Eq. (17) provides a mathematical definition of this distributed processing system.

$$y = \sum w_{ij} x_j + b_j \tag{17}$$

Where *xj* is the input trained node between the weights; moreover, input layers and hidden layers are represented by *wij*. The total input signals are considered 'n,' and the output node bias is denoted by *bj*. In most cases, the backpropagation (BP) method is used by an ANN to train itself. A standard method for determining the cost function is to

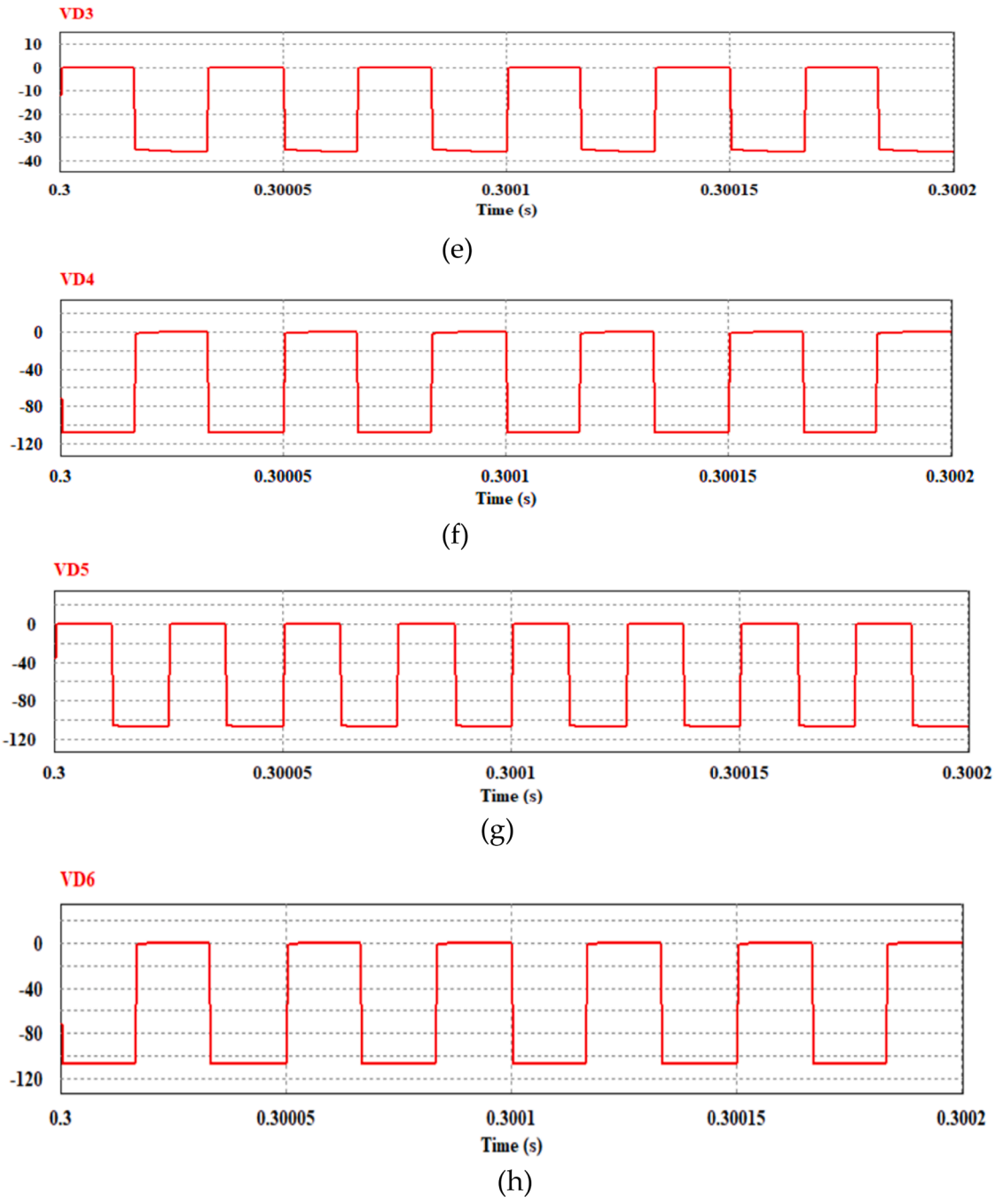

Fig. 14. (*continued*).

calculate the mean squared error (MSE) using Eq. (18) as,

$$MSE = \frac{1}{n}\sum_{i=1}^{n}\sum_{j=1}^{m}\left[Y_j(i) - T_j(i)\right]^2 \tag{18}$$

Where, m & n are denoted for the number of outputs and input data. Moreover, (i) is denoted for true output.

The sigmoid function outputs values between 0 and 1, making it suitable for applications where the duty cycle needs to be constrained within this range. The sigmoid function is given in the following equation

$$\sigma(x) = \frac{1}{1+e^x} \tag{19}$$

Using ANN, it can regulate the duty cycle by designing a network with a single hidden layer and activation functions such as sigmoid. This will give the output maps accurately to the range of 0 to 1. Utilise the mean squared error (MSE) loss function in order to get optimal results in any regression analysis. The initial learning rate is around 0.001, and if required, it may change using adaptive schedules. A batch size that strikes a compromise between the speed of convergence and the generalisation of the results is 5. Optimisation methods such as Adam, which adjusts the learning rate for each parameter and needs less tweaking than classic SGD, are used. The use of neural networks in this technique results in the provision of a solid framework for efficient duty cycle regulation. The classification of ANN used for simulation and experimentation is tabulated in the Table 1,

The ANN described in the hybrid approach generates IC using the input of the solar radiation received by the PV panel. Since the

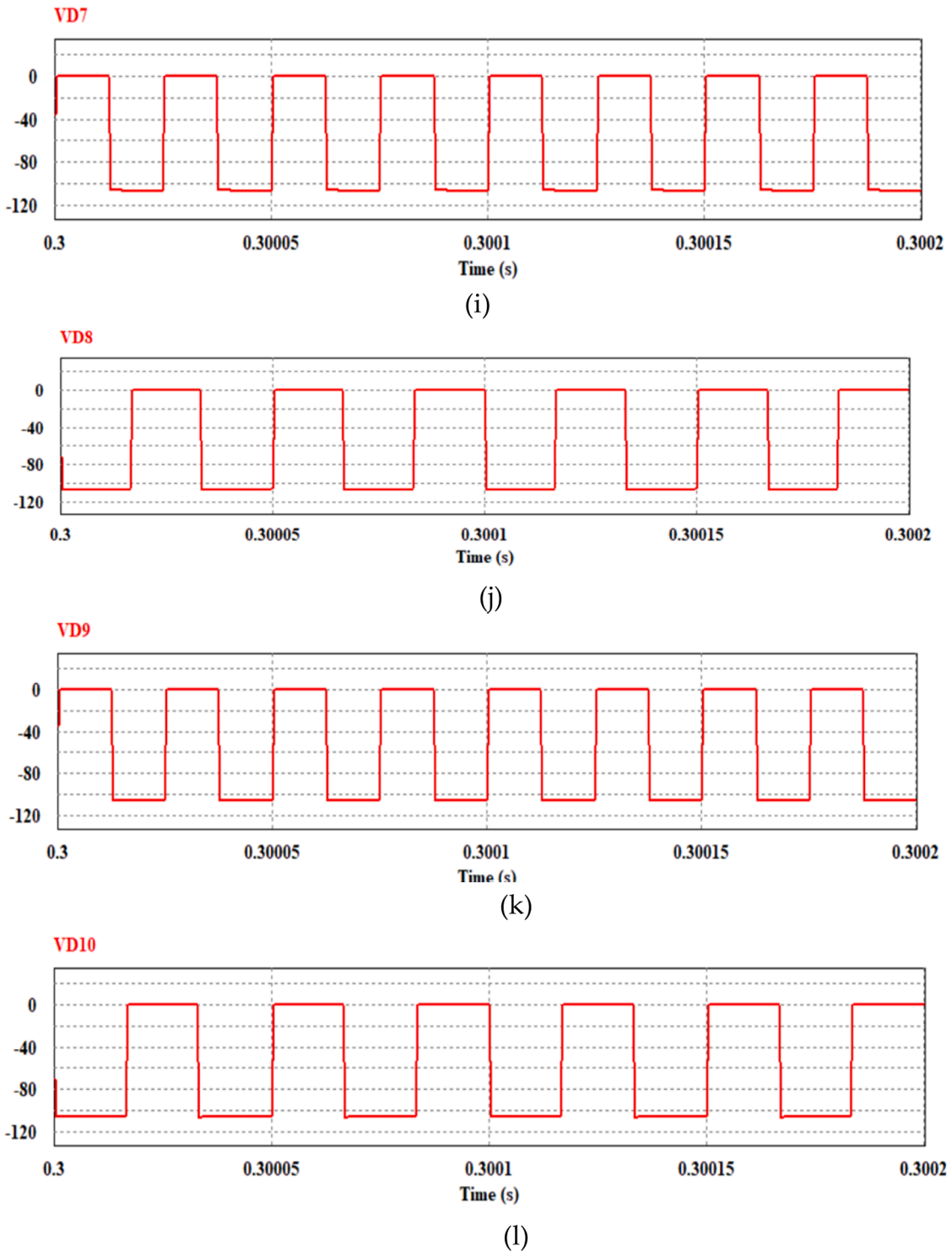

Fig. 14. (*continued*).

irradiance can vary, the array can produce many variants of partial shade patterns. Table 2 lists the ANN training settings for this approach. Fig. 9 displays the ANN's performance during training. According to the validation curve, the best performance was 0.00015 at epoch 34. According to the validation curve, the best performance was 0.00015 at epoch 34. Parameters used for the PV panel and ANN training are provided below

The switch carries out the primary action. The MPPT approach and the PID controller contribute to the switch's duty cycle formulation. Additionally, the suggested hybrid method combines the PSO method

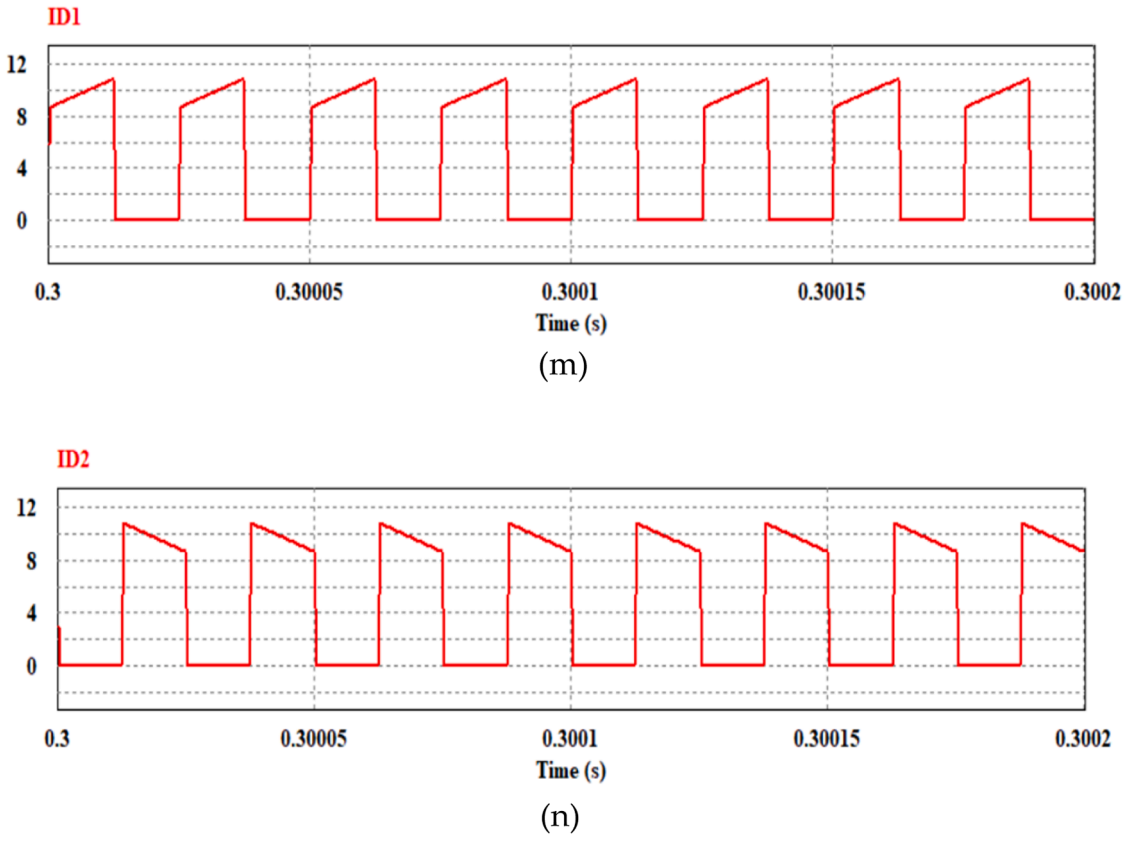

Fig. 14. (*continued*).

and ANN. One hundred populations have been chosen for optimization, and the maximum number of iterations is also 100. Maximum and minimum weight inertia is between 1 and 0.99. personal learning coefficient (C1) and global learning coefficient are 1.5 to 2, respectively.

4. Comparative analysis

Before comparing the proposed converter topology to others that have been considered, this one uses a high voltage gain topology and considers several topological considerations. As with the converters in [49,28,35], and [26], the one suggested has a continuous input supply with less ripple. An examination of existing topologies that are comparable to it has been conducted to confirm that the proposed converter improves performance. Table 2 compares the suggested converter functionality with other advanced topologies regarding voltage gain, normalized highest voltage stress, type of input current, and shared ground. The proposed converter has the maximum voltage gain compared to other converters; according to the voltage gain evaluation, the comparison is presented in Fig. 10a, demonstrating that the proposed configuration offers maximum gain. The duty ratio D must be more excellent than 25 % for the converter in [38] to obtain a higher gain. However, the converter's maximum D is restricted to 29.5 % [28].

Compared to other converters, the proposed one has extremely low switch voltage stress, as displayed in Fig. 10b. The switches in the converter only incur voltage stress of 76V for an output voltage of 429 V. Fig. 11a plots the normalized maximum diode voltage stress compared to the output voltage. It is noticeable that diode voltage stress is also dramatically reduced in the new structure.

The simulation has been carried out on other recent work with the MPPT controller to ensure maximum power tracking capability. All other topologies could function well when they are incorporated with photovoltaic sources. Fig. 11b shows the MPPT comparison of various configurations. It is proven from the simulation analysis that the proposed configuration outperforms others in terms of tracking MPP.

5. Results and discussion

5.1. Simulink analysis

The suggested converter is simulated in MATLAB/Simulink and PSIM Environment to verify the theoretical result. The solar panel is linked with a high-gain topology in the hybrid MPPT technique to develop the simulation model shown in Fig. 12. Under any circumstance, the converter draws the most power possible from the photovoltaic source. The boost converter's specifications used to perform the simulation are as follows:

$L_1=L_2=5$ mH
$C_1=C_2=300$ μF
$C_4=C_5=450$ μF
$C_5=C_6=C_7=550$ μF
$R_L=350$ Ω

The simulation setup and MPPT controller confirm the acceptability of the proposed topology results with and without MPPT. The simulation output stated the implimentabilty of the proposed configuration since it complies with the theoretical analysis. Table 3 summarises the performance comparison of various recently developed topologies with the proposed topology.

The circuit is simulated at the specified operating point using the above value. Fig. 13a shows the output voltage and switching pulse waveshape without utilizing MPPT for an input voltage of 36 V. Since the output voltage is 432 V, 1.22 A of load current flows at a 350 load. The inductor current is 9.7 A on average, and the ripple current is 3.4 A or 35 % of the average current, which is displayed in Fig. 13b. The voltage across capacitors is around 110 V. The capacitor raised the

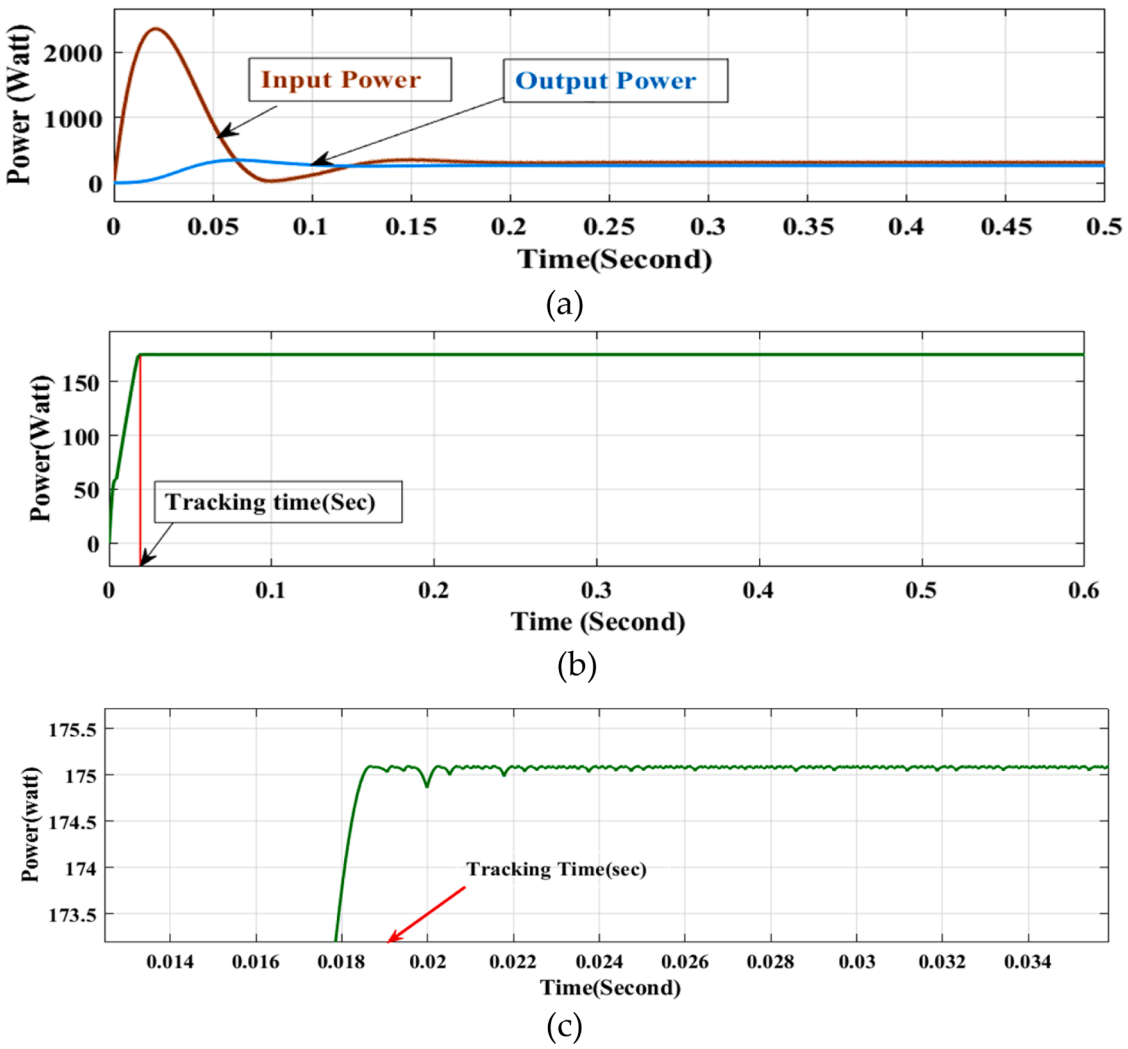

Fig. 15. Simulink result of proposed and topolgy with MPPT(a) input and output power (b) power tracked (c)zoom view of the tracking time.

voltage to 212 V, an exception from other capacitors.

Fig. 14 shows the voltage across the diodes used for simulation in the proposed configuration, and they all satisfy the theoretical waveform, as mentioned in Fig. 4. The MPPT controller's integration keeps the proposed circuit's efficiency, as depicted in Fig. 15(a), (b) shows the tracking time using a hybrid controller. Fig. 15(c) shows the zoom view of the output. The functionality of the hybrid MPPT is compared with that of conventional P&O MPPT. Fig. 16(a) shows that the hybrid algorithm can track power quickly and reduce the fluctuation around MPP. For a clear understanding, the zoom view is shown in Fig. 16(b).

5.2. Experimental study and analysis

To demonstrate the practicality of both MPPT methods, their performance is evaluated on a 175 W PV module. The project involves the real-time design of a standalone PV system that is coupled to a resistive load using a DC-DC converter. PV module ($P_m = 175W$, $V_m = 36.63V$, $I_m = 4.78A$) integrated with MPPT system, which is shown in experimental setup. Each method is tested in a controlled laboratory setting using illumination lamp settings to ensure the high rating system's performance. Fig. 17 shows the experimental setup that was used to examine both MPPT approaches as the solar irradiation was steadily increased from 0- 1000 W/m^2 and dcreesed from 1000 W/m^2 – 600 W/m^2 as,

When the PV system encountered conditions of gradually varying irradiance scenarios from 0–1000 W/m^2, the transient response of both MPPT methods was recorded on the screen of the digital storage oscilloscope (DSO), as shown in Fig. 18(a)-(b). P&O-based MPPT delivered electrical performance such as 169.6 W, 36.01 V, and 4.71A when the PV module was lit at 1000 W/m^2 (as shown in Fig. 18(a)), demonstrating its transient responsiveness under these conditions. Also, when comparing the P&O-based MPPT to the suggested PSO-ANN-based technique, the tracking time is noticeably longer for the former.

In addition, the transient response of PSO-ANN is displayed in Fig. 18 (b) at irradiance levels ranging from 0–1000 W/m^2 when the PV system is shaded. The result is an increase in the PV system output power of 171.11 W, voltage (36.1 V) and current as 4.74 A. Compared to traditional P&O-based MPPT, the tracking reaction time is also significantly lower.

In step-II, PV system encountered conditions of gradually varying irradiance scenarios from 1000–600 W/m^2, the transient response of both MPPT methods was recorded on DSO, as shown in Fig. 18(a)-(b).

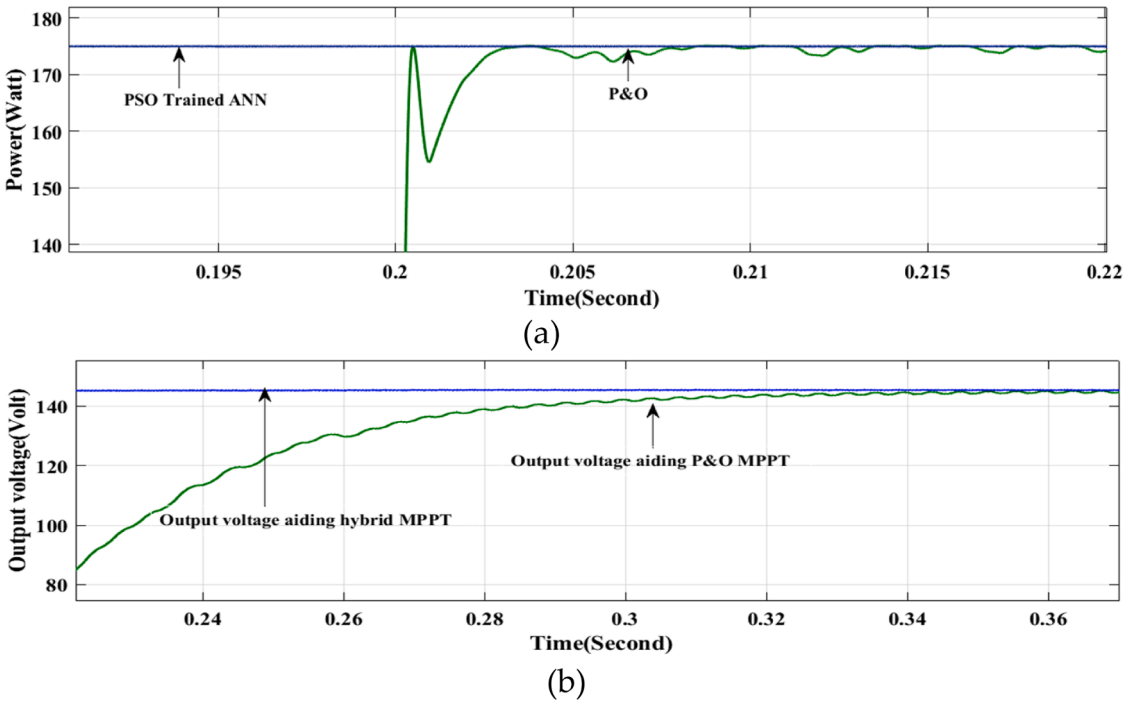

Fig. 16. Power tracking comparison using (a) PSO-ANN and P&O approach (b) zoom view of the comparison.

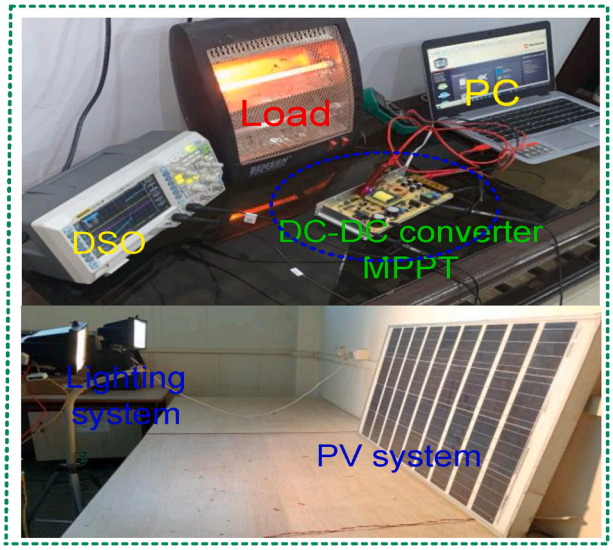

Fig. 17. Experimental setup for MPPT-assisted PV system.

P&O-based MPPT delivered electrical performance such as 134.6 W, 36.01 V, and 4.74A when the PV module was fixed at 600 W/m^2 (Fig. 18 (a)), demonstrating its transient responsiveness under these conditions. Also, when comparing the P&O-based MPPT to the suggested PSO-ANN-based technique, the tracking time is noticeably longer for the former.

In addition, the transient response of PSO-ANN is displayed in Fig. 18 (b) at irradiance levels ranging from 1000 W/m^2 – to 600 W/m^2 when the PV system is shaded. The result is an increase in the PV system performance in terms of power (136.8 W),voltage (36.1 V) and current (3.79). Performance is achhived for PSO-ANN is better than the conventional P&O based MPPT technique.

According to Table 4 & 5, PSO-ANN outperformed the traditional P&O-based MPPT method regarding output power while requiring less tracking time on a 175 W PV system. When comparing the P&O approach to a PSO-ANN-based MPPT strategy, the latter proved to be a more effective response to achieve the MPPT in less time.

In comparison to traditional P&O-based MPPT methods, PSO-ANN exhibits great accuracy, low implementation cost, and computational simplicity while still maintaining a high power output.

6. Conclusion

A non-isolated high-power quality DC-DC converter with high-power tracking MPPT controller is suggested in this research paper. Without utilizing transformer or an extremely high-duty cycle, it achieves a high voltage transformation ratio. Its control is made easy by the use of a single switch, which greatly reduces the cost. The following points are highlighted in the present study,

- The constructed DC-DC converter has a significant advantage over contemporary transformerless rivals in terms of efficiency, gain, and voltage stress. Additionally, employment of the hybrid algorithms enabled suggested structure to tracks the maximum power of the PV panel effectively.
- When compared to the P&O approach, the hybrid method dramatically reduced the tracking time with great efficiency. According to the comparative analysis and simulation results, the suggested converter achieves a high step-up ratio(12) and efficiency (95 %)with a low-duty cycle and a small number of components.
- During the experimental investigation, the PSO-ANN-based MPPT strategy demonstrated higher MPP values of 171.11 W under irradiance levels ranging from 0–1000 W/m2 compared to the P&O MPPT method of 169.6 W with a shorter tracking time response. Moreover, the PSO-ANN-based MPPT strategy shown higher MPP values of 136.8 W under irradiance levels ranging from 1000 W/m^2 to 600 W/m^2 compared to the conventional P&O MPPT method of 134.6 W.

This present study is based on simulation and experimental and will serve as a valuable resource for aspiring researchers in the fields of SPV-integrated MPPT techniques in the future.

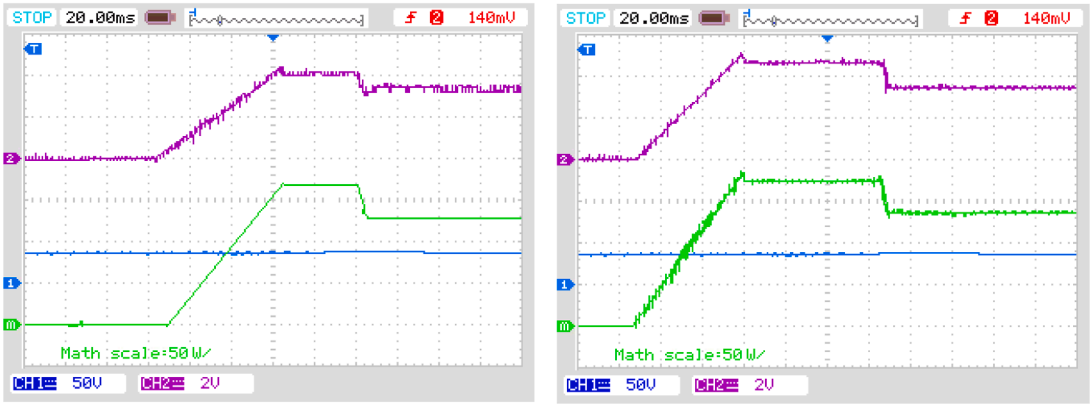

Fig. 18. Transient response of (a) P&O (b) PSO-ANN.

Table 4
P&O and PSO-ANN performance assessment for 175 W PV system at 600 W/m^2.

MPPT Techniques	Channel	Colour	Parameters	Scale	Performance at MPP at 1000 W/m^2
P&O	1	Blue	V (V)	50	36.01
	2	Pink	I (A)	2	4.71
	Math Scale (green)	Green	P (W)	50	169.6
PSO-ANN	1	Blue	V (V)	50	36.1
	2	Pink	I (A)	2	4.74
	Math Scale (green)	Green	P (W)	50	171.11

Table 5
P&O and PSO-ANN performance assessment for 175 W PV system under at 600 W/m^2.

MPPT Techniques	Channel	Colour	Parameters	Scale	Performance at MPP at 600 W/m^2
P&O	1	Blue	V (V)	50	36.01
	2	Pink	I (A)	2	3.74
	Math Scale (green)	Green	P (W)	50	134.6
PSO-ANN	1	Blue	V (V)	50	36.1 V
	2	Pink	I (A)	2	3.79 A
	Math Scale (green)	Green	P (W)	50	136.8 W

CRediT authorship contribution statement

Khadiza Akter: Writing – original draft, Validation, Methodology, Data curation, Conceptualization. **S.M.A. Motakabber:** Supervision, Methodology, Conceptualization. **A.H.M. Zahirul Alam:** Writing – review & editing, Supervision, Resources. **Siti Hajar Binti Yusoff:** Writing – review & editing, Supervision.

Declaration of competing interest

Authors have no conflict of interest regarding the present study.

Data availability

Data will be made available on request.

Acknowledgement

This work is supported by International Islamic Universit Engineering Merit Scholarshio 2021.

References

[1] Q. Sun, S. Chen, L. Chen, D. Ma, Quasi-Z-Source network-based hybrid power supply system for aluminum electrolysis industry, IEEE Trans. Ind. Informatics 13 (3) (2017) 1141–1151, https://doi.org/10.1109/TII.2016.2631129.
[2] O. Abdel-Rahim, A new high gain DC-DC converter with model-predictive-control based MPPT technique for photovoltaic systems, CPSS Trans. Power Electron. Appl. 5 (2) (2020) 191–200, https://doi.org/10.24295/cpsstpea.2020.00016.
[3] C. Rao, A. Hajjiah, M.A. El-Meligy, M. Sharaf, A.T. Soliman, M.A. Mohamed, A novel high-gain soft-switching DC-DC converter with improved PO MPPT for photovoltaic applications, IEEE Access 9 (2021) 58790–58806, https://doi.org/10.1109/ACCESS.2021.3072972.
[4] V.V. Reddy P, B.L. Narasimharaju, H.M. Suryawanshi, Implementation of dual control MPPT-based DC-DC converter fed solar PV power application, IEEE Trans. Ind. Electron. (2022), https://doi.org/10.1109/TIE.2022.3213891.
[5] A.M. Bazzi, P.T. Krein, Concerning maximum power point tracking for photovoltaic optimization using ripple-based extremum seeking control, IEEE Trans. Power Electron. 26 (6) (2011) 1611–1612, https://doi.org/10.1109/TPEL.2010.2093605.
[6] K. Kanathipan, J. Lam, A high voltage gain isolated PV Micro-converter with a single-voltage maximum power point tracking control loop for DC micro-grid systems, IEEE J. Emerg. Sel. Top. Ind. Electron. 3 (3) (2021) 755–765, https://doi.org/10.1109/jestie.2021.3130473.
[7] K. Sundareswaran, S. Peddapati, S. Palani, MPPT of PV systems under partial shaded conditions through a colony of flashing fireflies, IEEE Trans. Energy Convers. 29 (2) (2014) 463–472, https://doi.org/10.1109/TEC.2014.2298237.
[8] M.A. Elgendy, B. Zahawi, D.J. Atkinson, Assessment of perturb and observe MPPT algorithm implementation techniques for PV pumping applications, IEEE Trans. Sustain. Energy 3 (1) (2012) 21–33, https://doi.org/10.1109/TSTE.2011.2168245.
[9] A. Pandey, N. Dasgupta, A.K. Mukerjee, High-performance algorithms for drift avoidance and fast tracking in solar MPPT system, IEEE Trans. Energy Convers. 23 (2) (2008) 681–689, https://doi.org/10.1109/TEC.2007.914201.
[10] M.A.A. Mohd Zainuri, M.A. Mohd Radzi, A.C. Soh, N.A. Rahim, Development of adaptive perturb and observe-fuzzy control maximum power point tracking for photovoltaic boost dc-dc converter, IET Renew. Power Gener. 8 (2) (2014) 183–194, https://doi.org/10.1049/iet-rpg.2012.0362.

[11] M.A. Elgendy, B. Zahawi, D.J. Atkinson, Comparison of directly connected and constant voltage controlled photovoltaic pumping systems, IEEE Trans. Sustain. Energy 1 (3) (2010) 184–192, https://doi.org/10.1109/TSTE.2010.2052936.
[12] P.S. Samrat, F.F. Edwin, W. Xiao, Review of current sensorless maximum power point tracking technologies for photovoltaic power systems, in: *Proc. 2013 Int. Conf. Renew. Energy Res. Appl. ICRERA 2013*, no. October, 2013, pp. 862–867, https://doi.org/10.1109/ICRERA.2013.6749872.
[13] I.S. Kim, M.B. Kim, M.J. Youn, New maximum power point tracker using sliding-mode observer for estimation of solar array current in the grid-connected photovoltaic system, IEEE Trans. Ind. Electron. 53 (4) (2006) 1027–1035, https://doi.org/10.1109/TIE.2006.878331.
[14] X. Fang, X. Ding, S. Zhong, Y. Tian, Improved Quasi-Y-source DC-DC converter for renewable energy, CPSS Trans. Power Electron. Appl. 4 (2) (2019) 163–170, https://doi.org/10.24295/cpsstpea.2019.00016.
[15] S. Vighetti, J.P. Ferrieux, Y. Lembeye, Optimization and design of a cascaded DC/DC converter devoted to grid-connected photovoltaic systems, IEEE Trans. Power Electron. 27 (4) (2012) 2018–2027, https://doi.org/10.1109/TPEL.2011.2167159.
[16] D. Bao, A. Kumar, X. Pan, X. Xiong, A.R. Beig, S.K. Singh, Switched inductor double switch high gain DC-DC converter for renewable applications, IEEE Access 9 (2021) 14259–14270, https://doi.org/10.1109/ACCESS.2021.3051472.
[17] B.B. Converter and V. Khubchandani, "Extended switching-capacitor-based," vol. 4, no. 2, pp. 471–481, 2023.
[18] A. Rajabi, A. Rajaei, V.M. Tehrani, P. Dehghanian, J.M. Guerrero, B. Khan, A non-isolated high step-Up DC-DC converter using voltage lift technique: analysis, design, and implementation, IEEE Access 10 (2022) 6338–6347, https://doi.org/10.1109/ACCESS.2022.3141088.
[19] F. Mohammadzadeh Shahir, E. Babaei, M. Farsadi, Voltage-lift technique based nonisolated boost DC-DC converter: analysis and design, IEEE Trans. Power Electron. 33 (7) (2018) 5917–5926, https://doi.org/10.1109/TPEL.2017.2740843.
[20] J.C. Mayo-Maldonado, O.F. Ruiz-Martinez, G. Escobar, J.E. Valdez-Resendiz, T. M. Maupong, J.C. Rosas-Caro, Nonlinear stabilizing control design for DC-DC converters using lifted models, IEEE Trans. Ind. Electron. 68 (11) (2021) 10772–10783, https://doi.org/10.1109/TIE.2020.3031530.
[21] G. Zhang, B. Zhang, Z. Li, D. Qiu, L. Yang, W.A. Halang, A 3-Z-network boost converter, IEEE Trans. Ind. Electron. 62 (1) (2015) 278–288, https://doi.org/10.1109/TIE.2014.2326990.
[22] S.A. Ansari, J.S. Moghani, A novel high voltage gain noncoupled inductor SEPIC converter, IEEE Trans. Ind. Electron. 66 (9) (2019) 7099–7108, https://doi.org/10.1109/TIE.2018.2878127.
[23] A. Andrade, T. Faistel, R. Guisso, A. Toebe, Hybrid high voltage gain transformerless DC-DC converter, IEEE Trans. Ind. Electron. 69 (3) (2022) 2470–2479, https://doi.org/10.1109/TIE.2021.3066939.
[24] H. Gholizadeh, S.A. Gorji, D. Sera, A quadratic buck-boost converter with continuous input and output currents, IEEE Access 11 (2023) 22376–22393, https://doi.org/10.1109/ACCESS.2023.3253102. March.
[25] T. Jalilzadeh, N. Rostami, E. Babaei, M. Maalandish, Nonisolated topology for high step-up DC-DC converters, IEEE J. Emerg. Sel. Top. Power Electron. 11 (1) (2023) 1154–1168, https://doi.org/10.1109/JESTPE.2018.2849096.
[26] S. Gopinathan, V.S. Rao, K. Sundaramoorthy, Family of non-isolated quadratic high gain DC-DC converters based on extended capacitor-diode network for renewable energy source integration, IEEE J. Emerg. Sel. Top. Power Electron. 10 (5) (2022) 6218–6230, https://doi.org/10.1109/JESTPE.2022.3167283.
[27] S. Gopinathan, V.S. Rao, Enhanced voltage gain boost DC-DC converter with reduced voltage stress and core saturation, IEEE Trans. Circuits Syst. II Express Briefs (2023), https://doi.org/10.1109/TCSII.2023.3252721. Ccm.
[28] K. Kamalinejad, H. Iman-Eini, S.H. Aleyasin, M.Abbasi Ghadi, A novel non-isolated buck-boost DC-DC converter with low voltage stress on components, IEEE J. Emerg. Sel. Top. Ind. Electron. 4 (2) (2023) 1–10, https://doi.org/10.1109/jestie.2023.3239821.
[29] S.D.C.D.C. Converters, "Nonisolated topology for high," vol. 11, no. 1, pp. 1154–1168, 2023.
[30] M. Rezaie, V. Abbasi, Ultrahigh Step-Up DC-DC converter composed of two stages boost converter, coupled inductor, and multiplier cell, IEEE Trans. Ind. Electron. 69 (6) (2022) 5867–5878, https://doi.org/10.1109/TIE.2021.3091916.
[31] D.C.D.C. Converter and L.G. Salem, "A series-parallel switched-photovoltaic," vol. 58, no. 3, pp. 742–756, 2023.
[32] X. Wu, M. Yang, M. Zhou, Y. Zhang, J. Fu, A novel high-gain DC-DC converter applied in fuel cell vehicles, IEEE Trans. Veh. Technol. 69 (11) (2020) 12763–12774, https://doi.org/10.1109/TVT.2020.3023545.
[33] M. Veerachary, P. Kumar, Analysis and design of quasi-z-source equivalent DC-DC boost converters, IEEE Trans. Ind. Appl. 56 (6) (2020) 6642–6656, https://doi.org/10.1109/TIA.2020.3021372.
[34] M.M. Haji-Esmaeili, E. Babaei, M. Sabahi, High Step-Up Quasi-Z source DC-DC converter, IEEE Trans. Power Electron. 33 (12) (2018) 10563–10571, https://doi.org/10.1109/TPEL.2018.2810884.
[35] R. Rahimi, S. Habibi, M. Ferdowsi, P. Shamsi, Z-source-based high step-up DC-DC converters for photovoltaic applications, IEEE J. Emerg. Sel. Top. Power Electron. 10 (4) (2022) 4783–4796, https://doi.org/10.1109/JESTPE.2021.3131996.
[36] M. Veerachary, P. Sen, Dual-switch enhanced gain boost DC-DC converters, IEEE Trans. Ind. Appl. 58 (4) (2022) 4903–4913, https://doi.org/10.1109/TIA.2022.3171533.
[37] S. Miao, W. Liu, J. Gao, Single-inductor boost converter with ultrahigh step-up gain, lower switches voltage stress, continuous input current, and common grounded structure, IEEE Trans. Power Electron. 36 (7) (2021) 7841–7852, https://doi.org/10.1109/TPEL.2020.3047660.
[38] A. Kumar, et al., A High voltage gain dc-dc converter with common grounding for fuel cell vehicle, IEEE Trans. Veh. Technol. 69 (8) (2020) 8290–8304, https://doi.org/10.1109/TVT.2020.2994618.
[39] M.K. Nguyen, T.D. Duong, Y.C. Lim, Switched-capacitor-based dual-switch high-boost DC-DC converter, IEEE Trans. Power Electron. 33 (5) (2018) 4181–4189, https://doi.org/10.1109/TPEL.2017.2719040.
[40] K.Y. Yap, C.R. Sarimuthu, J.M.Y. Lim, Artificial intelligence based MPPT techniques for solar power system: a review, J. Mod. Power Syst. Clean Energy 8 (6) (2020) 1043–1059, https://doi.org/10.35833/MPCE.2020.000159.
[41] K. J, F. SY, Modeling of a photovoltaic array in matlab simulink and maximum power point tracking using neural network, J. Electr. Electron. Syst. 07 (03) (2018) 1–8, https://doi.org/10.4172/2332-0796.1000263.
[42] E. Bouchetob, B. Nadji, Using ANN based MPPT controller to increase PV central performance, in: 2022 2nd Int. Conf. Adv. Electr. Eng. ICAEE 2022, 2022, pp. 1–6, https://doi.org/10.1109/ICAEE53772.2022.9961982.
[43] R. Rq et al., "' LIIHUHQW: HDWKHU & RQGLWLRQV," vol. 5, pp. 3–8.
[44] M. Motakabbir Rahman, M. Shahidul Islam, PSO and ANN based hybrid MPPT algorithm for photovoltaic array under partial shading condition, Eng. Int. 8 (1) (2020) 9–24.
[45] R. Rahimi, S. Habibi, M. Ferdowsi, P. Shamsi, An interleaved quadratic high Step-Up DC-DC converter with coupled inductor, IEEE Open J. Power Electron. 2 (2021) 647–658, https://doi.org/10.1109/OJPEL.2021.3133911. November.
[46] M.L. Alghaythi, R.M. O'Connell, N.E. Islam, M.M.S. Khan, J.M. Guerrero, A high step-up interleaved DC-DC converter with voltage multiplier and coupled inductors for renewable energy systems, IEEE Access 8 (2020) 123165–123174, https://doi.org/10.1109/ACCESS.2020.3007137.
[47] X. Hu, X. Liu, Y. Zhang, Z. Yu, S. Jiang, A Hybrid cascaded high Step-Up DC-DC converter with ultralow voltage stress, IEEE J. Emerg. Sel. Top. Power Electron. 9 (2) (2021) 1824–1836, https://doi.org/10.1109/JESTPE.2020.2975856.
[48] T. Liu, M. Lin, J. Ai, High step-up interleaved dc-dc converter with asymmetric voltage multiplier cell and coupled inductor, IEEE J. Emerg. Sel. Top. Power Electron. 8 (4) (2020) 4209–4222, https://doi.org/10.1109/JESTPE.2019.2931634.
[49] P. Manoharan, et al., Improved perturb and observation maximum power point tracking technique for solar photovoltaic power generation systems, IEEE Syst. J. 15 (2) (2021) 3024–3035, https://doi.org/10.1109/JSYST.2020.3003255.

Khadiza Akter received an engineering degree in Electrical and Electronic Engineering from the International University of Business Agriculture Technology (IUBAT) of Bangladesh in 2011, She received her Master's degree in Power electronics from the Faculty of EEE from Islamic University of Technology (IUT) in 2018. She worked as an Assistant Professor at IUBAT from January 2019 to January 2022. Previously she served as a Lecturer at the same department from March 18, 2012 and subsequently promoted to Senior Lecturer and Assistant Professor. Currently, she is working as Research Assistant at the Laboratory of Power electronics and renewable energy research-Department of Electrical and Computer Engineering, International Islamic University Malaysia (IIUM). Her research interests include power electronics, renewable energy, and batteries. She can be contacted at email: khadiza@iubat.edu.

S.M.A Motakabber is an Associate Professor at the Department of Electrical and Computer Engineering, International Islamic University Malaysia, Malaysia, received the BSc (Honours) and Master's degrees from the University of Rajshahi in 1986 and 1987, and pH. D from University Kebangsaan Malaysia in 2011. He served as a scientific officer at the Bangladesh Atomic Energy Commission, and Bangladesh Scientific and Industrial Research, Dhaka from 1991–1992 and 1992–1993, respectively. He started his teaching career as a lecturer in the Department of Applied Physics and Electronics, University of Rajshahi in 1993. The following year he was appointed an Assistant Professor in the same department. He joined as an Associate Professor in the Department of Computer and Communication Engineering at International Islamic University Chittagong in 2003; also served as Head of the Department and Dean of the Engineering Faculty. He can be contacted at email: amotakabber@iium.edu.my.

AHM Zahirul Alam received the B.*Sc*. and M.*Sc*. degrees in Electrical and Electronic Engineering from Bangladesh University of Engineering and Technology (BUET) in 1984 and 1987, respectively. He obtained his Doctor of Engineering degree from Kanazawa University, Japan in 1996. He was working as a faculty member in BUET from 1985 to 1991 and from 1996 to March 2002. He became a professor in BUET in 1999. He worked in the MIRAI project in Low-k group in Advanced Semiconductor Research Center, Tsukuba, Japan through Japan Science and Technology fellow from April 2002 to October 2003. He is currently serving as a Professor of Electrical and Computer Engineering Department, Faculty of Engineering, International Islamic University Malaysia (IIUM). His research interest includes electronic device modeling and fabrication, RF devices and MEMS, Energy harvesting system, antenna and communication devices. He can be contacted at email: zahirulalam@iium.edu.my.

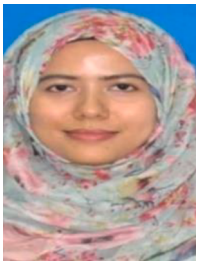

Siti Hajar Binte Yousoff a former student of Kolej Yayasan UEM (KYUEM), Lembah Beringin. She obtained first class with honours in her MEng Degree (First Class Hons) (Electrical Engineering) and Doctor of Philosophy in Electrical& Electronic Engineering from the University of Nottingham, UK. Currently, she is attached to the Department of Electrical and Computer Engineering. Her specialization is in the area of power electronics and nonlinear control systems. Her research interests include wireless power transfer in electric vehicles (EV), energy management systems, renewable energy, microgrid, and IoT. He can be contacted at email: sitiyusoff@iium.edu.my.